Evolution of the stratospheric polar vortex edge intensity and duration in the Southern hemisphere over the 1979 – 2020 period

Audrey Lecouffe[1], Sophie Godin-Beekmann[1], Andrea Pazmiño[1], and Alain Haucheorne[1]

[1]LATMOS/IPSL, UVSQ, Sorbonne Université, CNRS, Paris, France

Correspondence: Audrey Lecouffe (audrey.lecouffe@latmos.ipsl.fr)

Abstract. The intensity and position of the Southern Hemisphere stratospheric polar vortex edge is evaluated as a function of equivalent latitude over the 1979 - 2020 period on three isentropic levels (475K, 550K and 675K) from ECMWF ERA-Interim reanalysis. The study also includes an analysis of the onset and breakup dates of the polar vortex, which are determined from wind thresholds (e.g. 15.2 m.s^{-1}, 20 m.s^{-1} and 25 m.s^{-1}) along the vortex edge. The vortex edge is stronger in late winter,

5   over September - October - November with the period of strongest intensity occurring later at the lowermost level. A lower variability of the edge position is observed during the same period. Long-term increase of the vortex edge intensity and break-up date is observed over the 1979 - 1999 period, linked to the increase of the ozone hole. Long-term decrease of the vortex onset date related to the 25 m.s^{-1} wind threshold is also observed at 475K during this period. The solar cycle and to a lower extent the quasi-biennal oscillation (QBO) and El Niño Southern Oscillation (ENSO) modulate the inter-annual evolution of

10 the strength of the vortex edge and the vortex breakup dates. Stronger vortex edge and longer vortex duration is observed in solar minimum (minSC) years, with the QBO and ENSO further modulating the solar cycle influence, especially at 475K and 550K: during West QBO (wQBO) phases, the difference between vortex edge intensity for minSC and maxSC years is smaller than during East QBO (eQBO) phases. The polar vortex edge is stronger and lasts longer for maxSC/wQBO years than for maxSC/eQBO years. ENSO has a weaker impact but the vortex edge is somewhat stronger during cold ENSO phases for both

15 minSC and maxSC years.

1   Introduction

The stratospheric polar vortex is a seasonal low-pressure system characterized by a strong wind belt that isolates polar air from lower latitudes. It appears due to the seasonal cooling associated with the decrease of solar radiation above the pole. As the incident solar energy decreases, and the gradient of temperature between the pole and the tropics becomes stronger, the

20 strength of the stratospheric westerly winds increases. When the winds reach a critical value, a large-scale vortex is formed, which extends from the lowermost stratosphere to the stratopause. Depending on altitude, the maximum area encompassed by the polar vortex exceeds millions of square kilometers (NOAA, 2021). Above an altitude of about 14 km, the vortex edge region is stable and constitutes a powerful barrier, preventing mixing of cold polar air with warmer air masses from lower latitudes. Over Antarctica, the polar vortex is generally present from May until the end of November. Conversely, the less

25 stable Arctic polar vortex forms in November and lasts until the end of February or early April, depending on the year. The

stratospheric polar vortices have been the subject of studies linked to the depletion of the ozone layer, which started in the late 1970 (Farman et al., 1985; Schoeberl and Hartmann, 1991). In the Southern Hemisphere, the ozone hole, defined as an area with total ozone values less than 220 DU, has become a recurring seasonal phenomenon. Ozone destruction begins in late winter, close to the edge region of the polar vortex, as solar radiation increases over the Pole. The destruction of ozone

5   inside the vortex accelerates from late August until late September or early October, reaching an almost total destruction of ozone in the lower stratosphere. The depletion of the ozone layer is caused by anthropogenic emission of ozone depleting substances (ODS - mainly chlorofluorocarbons and halons and their industrial substitutes), which enhances ozone destruction cycles by halogen compounds. This depletion is largest in the polar vortex due to the activation of chlorine species through heterogeneous reactions that take place at the surface of polar stratospheric clouds (PSCs) which form in the cold polar vortex

10   (Solomon, 1999). The increase in solar radiation over the Pole at the end of winter triggers rapid chemical cycles which quickly destroy ozone, leading to the appearance of the well-known ozone hole over Antarctica (e.g. WMO, 2018). PSCs are found to be much more abundant in the Antarctic polar vortex as compared to the Arctic polar vortex due to the increased stability of the southern polar vortex. As a result of the asymmetry in polar vortices intensity, the southern vortex experiences much colder temperatures in winter, which results in stronger ozone depletion over a large area (the so-called ozone hole). By the end of

15   spring, stratospheric temperatures increases, the polar vortex breaks up and ozone depleted air masses dilute in the Southern Hemisphere. From one year to the next, the severity of the ozone hole will thus depend on the strength of the polar vortex, its minimum temperatures and duration. The future recovery of the ozone layer and disappearance of the ozone hole depends on the evolution of the polar vortex under the influence of both the decrease of ODS abundance in the stratosphere and the increase of greenhouse gases (GHG) as both phenomena impact radiative, dynamical and chemical processes in the stratosphere.

20   The inner vortex is characterized by high absolute values of potential vorticity (PV). As this parameter is conserved on isentropic surfaces during weeks, the mapping of PV on such surfaces is one of the primary diagnostic tools for the analysis of dynamical processes in the stratosphere and inside the polar vortex. McIntyre and Palmer (1983) first represented daily PV global maps of isentropic surfaces, demonstrating a material separation in the stratosphere between the main vortex, character- ized by high absolute PV values, the surf zone, characterized by a weak absolute PV values, and a zone of strong meridional

25   PV gradient in between: the so-called vortex boundary or vortex edge, which is an area of low mixing representing a dynamical barrier to air masses exchanges. Numerous studies on the vortex boundary definition have been performed. Nash et al. (1996) defined the vortex edge as the location of the maximum PV gradient as a function of equivalent latitude (EL), weighted by the wind module. This is the method used in this study. The equivalent latitude is a parameter defined from the PV maximum within the vortex, e.g. Butchart and Remsberg (1986). Nakamura (1996) has developed the effective diffusivity diagnostic,

30   which is applied on tracers to identify transport barriers and regions of mixing. Hauchecorne et al. (2002) used this method to quantify the transport of polar vortex air to mid-latitudes, as well as to evaluate the polar vortex barrier intensity. The method of elliptical diagnostics of a contour used by Waugh (1997), consists in fitting an ellipse to the contour of a parameter. It subsequently determines several variables of this ellipse, for example latitude and longitude of the center, the equivalent lat- itude, or its orientation. It is possible to calculate the elliptical diagnostics of a contour of conservative tracers such as PV

35   or long-lived chemical species around the polar vortex edge region (Waugh and Randel, 1999). The vortex forms in autumn,

intensifies throughout the winter and disappears in spring/summer. Its overall strength is variable from one year to the next. Different works have analyzed the inter-annual variability of the polar vortex induced by forcings such as the solar flux (SF), Quasi-Biennial Oscillation (QBO) and El Niño Southern Oscillation (ENSO), particularly in the Northern Hemisphere. QBO is a quasi-periodic oscillation of the equatorial zonal wind between easterlies and westerlies. Holton and Tan (1980) made a

5   composite study of zonal wind in the Northern Hemisphere at 50hPa from 1962 to 1977 based on the different phases of QBO. They showed that the vortex is less disturbed during the West phase of the QBO (wQBO) at 50hPa than during the East phase (eQBO). Labitzke and Van Loon (1988) evaluated the temperature and strength of the Arctic polar vortex according to the solar cycle and the QBO. They found that the vortex is warm and weak during solar maxima/eQBO phases, and cold and strong during solar minima/wQBO phases at 50 hPa. Then, Baldwin and Dunkerton (1998) showed over a period of 18 years, that

10   the Antarctic polar vortex at 10hPa is slightly colder during wQBO. ENSO is an irregular oscillation in winds and sea surface temperatures over the tropical eastern Pacific Ocean, affecting the climate of the tropics and subtropics. It influences also other climatic parameters such as precipitations worldwide and ozone levels in the lower stratosphere (WMO, 2018). Several methods have been suggested in order to determine the onset and breakup dates of the polar vortices. They are based on a minimum area computed from equivalent latitudes (Manney et al. 1994; Zhou et al. 2000) or wind speed thresholds at the edge of the

15   vortex (e.g. Nash et al. 1996). Manney et al. (1994) and Zhou et al. (2000) consider that the vortex breaks down and disappears when its size falls below 1% of the Earth's surface, or when its edge position is larger than 78.5°EL. More recently, Millan et al. (2020) compared the polar vortex evolution with different reanalyses, including ERA-Interim. Results showed that all reanalyses where in agreement with the reanalysis ensemble mean (REM), which shows that we can be confident with the ERA-Interim reanalyses for our study.

20   The objective of this paper is to analyze the long-term evolution of the intensity, position and duration of the Southern polar vortex edge as a function of equivalent latitude over several decades (1979 – 2020). ERA-Interim reanalyses and operational data from the European Centre for Medium-Range Weather Forecast (ECMWF) are used for the study, which includes an evaluation of the onset and breakup dates of the polar vortex over the period. At an inter-annual scale, the signature of the 11-year solar cycle, QBO and ENSO, is evaluated on the vortex edge evolution.

25   The paper is organized as follows. Section 2 presents the ECMWF dataset and the data sources of the forcings (SF, QBO, and ENSO) used for the analysis of inter-annual variability of the polar vortex edge. Section 3 describes the methods used in the study, such as the MIMOSA (Modélisation Isentrope du transport Méso-échelle de l'Ozone Stratosphérique par Advection) model (Hauchecorne et al., 2002), which is used to construct the PV maps as a function of potential temperature and equivalent latitude. The methods used for the vortex edge characterization and for determining the onset and breakup dates of the polar

30   vortex are also discussed in this section. Section 4 presents the statistical analysis of the annual evolution of the vortex edge over the studied period as well as its inter-annual evolution, related to the SF, QBO and ENSO forcings, while results on the inter-annual evolution of the vortex onset and breakup dates are given in Section 5. Further discussion of the results and perspective of the study are presented in Section 6.

2 Data

2.1 Potential vorticity fields

PV fields are calculated from ECMWF ERA-Interim reanalysis [1] (Dee et al., 2011). As these reanalyses end in August 2019, we used the operational data from ECMWF from September 2019 until December 2020. They are characterized by a resolution

5 of 1.125° latitude x 1.125° longitude. ERA-Interim temperature, geopotential and wind data are the inputs for the MIMOSA model, which computes PV and EL fields on different isentropic surfaces with a resolution of 0.3° latitude x 0.3° longitude, using a polar projection centered on the South. The MIMOSA model is a three-dimensional high-resolution PV advection model (Hauchecorne et al., 2002) which has been used to analyze, among other studies, the permeability of the southern polar vortex to volcanic aerosols from Cerro Hudson and Mount Pinatubo eruptions in 1991 (Godin et al., 2001), to predict the

10 extension in the lower mid-latitude stratosphere of polar and subtropical air masses (Heese et al., 2001), or to evaluate average total ozone evolution within the Antarctic vortex with PV fields simulated by the model, used to determine the vortex position in Pazmino et al. (2018). For this study, PV fields are computed at 675K, 550K and 475K isentropic surfaces.

2.2 Forcings of interannual variability

Forcings considered for the analyses of the inter-annual variability of the vortex edge are described in Table 1. For the solar

15 flux, we are mainly interested in the variability induced by the 11-year solar cycle. The F10.7 solar flux data record related to this cycle covers six solar cycles, including those covering our study period, the last four. It correlates well with the 11-year sunspot cycle (Mishra et al., 2005, Tiwari and Kumar, 2018) and has been used frequently as a proxy for solar activity (e.g. Solomon, 1999; Gray, 2003; Pazmino et al., 2018). It is defined in solar flux units (1 sfu = 10^{-22} W.m^{-2}.Hz^{-1}). For our study, we averaged the 10.7-cm solar flux over the May - November period, which corresponds to the time period when the Southern

20 polar vortex is formed, in order to analyse its impact on the vortex edge. Data were obtained for the 21th to the 24th solar cycle (1976 to 2020). Years characterized by minimum and maximum solar intensity were selected from the difference of maximum and minimum intensity of each cycle. The minimum (maximum) intensity threshold was defined as the lower (upper) third of this difference, so that the minimum and maximum thresholds are different for each cycle. The selection results in 15 maximum solar (maxSC) years and 20 minimum solar (minSC) years over the whole studied period. In order to investigate the influence

25 of QBO on the polar vortex, we used Singapore monthly mean zonal wind at the 50hPa level, and averaged this parameter each year during the same period as for the solar cycle. QBO is sorted by negative phase for East QBO (eQBO) with 19 years and positive phase for West QBO (wQBO) with 23 years. In the case of El Niño Southern Oscillation, the Multivariate ENSO Index (MEI) version 2 was used in this study. It correspond to the combination of empirical orthogonal function (EOF) of sea level pressure (SLP), sea surface temperature (SST), zonal and meridional components of surface wind and outgoing longwave

30 radiation in the tropical Pacific basin. Data are for bi-monthly periods to take into account the seasonality of ENSO (see data availability [4]). As for SC and QBO, we averaged these data during the May - November period. Then mean ENSO is sorted to distinguish La Niña, characterized by a negative MEI (cold ENSO), and El Niño, characterized by a positive MEI (warm ENSO). The studied period is characterized by 21 wENSO and 21 cENSO years.

Table 1. Proxies: source, characteristics and period.

Proxy	Source	Characteristics	Period
SF	Dominion Radio Astrophysical Observatory (National Research Council Canada) [2]	Monthly mean solar flux at 10.7-cm	May - November
QBO	Institute of Meteorology (Freie Universität Berlin) [3]	Monthly mean quasi-biennial oscillation at 50hPa	May - November
ENSO	NOAA Earth System Research Laboratory [4]	Bi-monthly Multivariate ENSO index (MEI.v2)	May - November

3 Methods

3.1 Vortex edge characterization

As mentioned in the introduction, the vortex edge is characterized by a strong PV gradient. To represent the vortex edge position, the method described in Nash et al. (1996) is used, which consists in determining the position of the edge from the maximum PV gradient weighted by the wind module as a function of EL. The maximum gradient is evaluated in the [-85°, -40°EL] range in order to avoid high PV values at the pole and disturbances with the equatorial barrier. The position of the edge is defined by the EL of the $max(dPV/dEL \times W(EL)[-85°, -40°EL])$ where W correspond to the wind module.

3.2 Onset and Breakup determination

Several methods have been used in order to determine the onset and breakup dates of the polar vortex in the Northern hemisphere (NH), as mentioned previously. Manney et al. (1994) first determined that the breakup date corresponds to the date when the EL of a chosen PV contour at the 465K level is greater than 80°, using PV data from the National Centers for Environmental Prediction and the National Center for Atmospheric Research (NCEP/NCAR) reanalyses. From a given PV contour, the authors determined that if the corresponding EL position is poleward 80°LE, then the vortex is not well formed. This defines the duration of the polar vortex. Subsequently, using wind fields in addition to the PV gradient as a function of EL, Nash et al. (1996) considered that the vortex is well formed at 450K when the wind module along the vortex edge is equal to or greater than 15.2 m.s^{-1}. They also used the 3.2 m.s^{-1} standard deviation interval to provide a range of dates during which the vortex forms and breaks. Then Waugh et al. (1999) analyzed the breakup date of the Arctic and Antarctic polar vortices using NCEP data for the 1958-1999 period. They showed a tendency of extension of the breakup date after 1979 in the Antarctic that could be linked to the Antarctic ozone depletion due to radiative processes induced by the lower ozone levels within the vortex. Zhou et al. (2000) used the same method as Manney et al. (1994) and compared the vortex breakup dates in the 1990s with those of the 1980s based on NCEP data, considering that the vortex breaks and disappears when its size falls below 1% of the Earth's

surface. The authors demonstrated that the vortex lasted two weeks longer in the 1991-1998 period than in the 1979 - 1984 period in the Southern Hemisphere. The authors joined other studies in concluding that the vortex lifetime is influenced by the ozone depletion during spring. Still in the Southern Hemisphere, Akiyoshi et al. (2009) used the same method as Nash et al. (1996) and added threshold values of 20 and 25 $m.s^{-1}$ to compare variations of breakup dates in model and observations over

5 the 1980–2004 period. In this study, we use the Nash et al. (1996) method to determine the vortex onset and breakup dates, used also in WMO (2019), with three threshold values (15 $m.s^{-1}$, 20 $m.s^{-1}$ and 25 $m.s^{-1}$) following Akiyoshi et al. (2009).

4 Statistical analysis of the evolution of the Polar vortex edge throughout the winter

4.1 Intensity of the vortex edge

The statistical analysis of the evolution of the vortex edge intensity throughout the winter from 1979 to 2020 at the 675K,

10 550K and 475K isentropic surfaces is shown in Figure 1, which displays the maximum PV gradient smoothed by 5 days running mean, as a function of EL from May to December. In each panel, the black bold curve represents the median values and blue filled areas indicate values between 20th and 80th percentiles. Thin dark lines are the overall maximum and minimum daily values over the 1979 - 2020 period. Data are considered every year between the onset and the breakup dates of the vortex (see section 5) and the percentiles, median and overall extrema are plotted for days with 3 years or more of data. The statistical

15 parameters with at least 3 years of data are obtained until day 343, 354 and 361 at 675K, 550K and 475K respectively. Results show that the vortex is systematically present on May 1st, and reaches its maximum intensity during different periods of the winter depending on the level, e.g. later at the lower levels. It is reached from September to late October at 675K with a median peak value of 20.8 PV units/°EL in October, from September to early November at 550K with a peak value of 7.8 PV units/°EL at the beginning of October, and later for 475K during the first half of November with a peak value of 3.9 PV units/°EL. This

20 period of maximum intensity is also characterized by a larger variability (as seen from the maximum and minimum curves, especially in for the lower isentropic levels). Depending on the year and the level, the vortex breaks up between mid-October and the end of December at the latest.
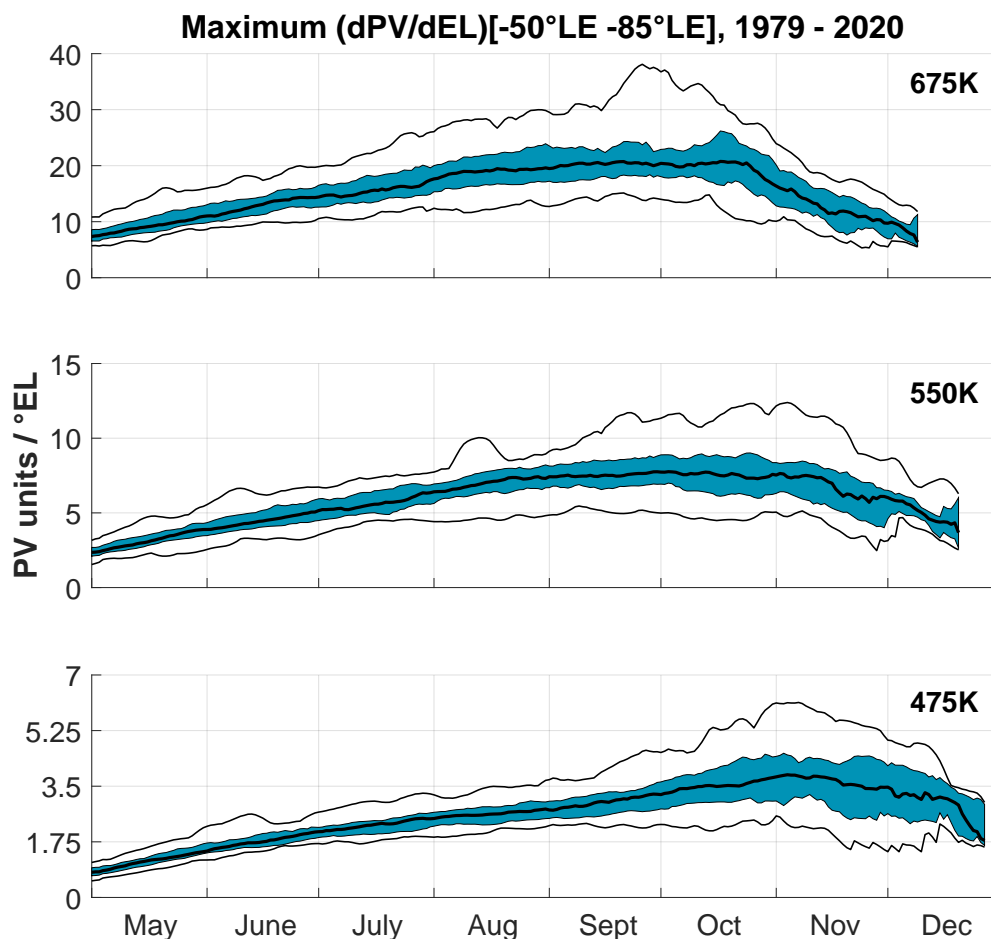
Figure 1. Evolution of daily maximum PV gradient for the 1979 - 2020 period, from top to bottom: 675K, 550K and 475K. Median value are represented by black bold curve. Blue filled areas show values between 20 and 80 percentiles, while thin black curves represent the maximum and minimum values over the period.

Figure 2 represents the statistical evolution of the vortex edge position in EL as described in Figure 1 for the PV gradient. For this parameter, medians and percentiles curves show a similar behavior for the various levels from May to late September for all levels. The maximal polar vortex edge position is reached between mid-July and late August at 675K, between mid-July and mid-August at 550K and between mid-August and September at 475K, with respective median average values of -57.3°EL, -57.8°EL and -58.4°EL. The overall maxima and minima show clearly the vortex's large area reduction due to the major warming in 2002 during October. It is less pronounced at 475K where the edge position decreased to a minimum of -67.8°EL, compared to -76.3°EL and -71°EL at 675K and 550K, respectively (e.g. Hoppel et al. 2003). The variability in vortex area decreases for all levels during the period of maximum edge intensity period: between the 20th and 80th percentiles

it reduces to 3.7°EL difference in October at 675K, and 3.1°EL at the 550K and 475K levels compared to 4.6°EL, 5.4°EL and 5.2°EL from top to bottom in August.
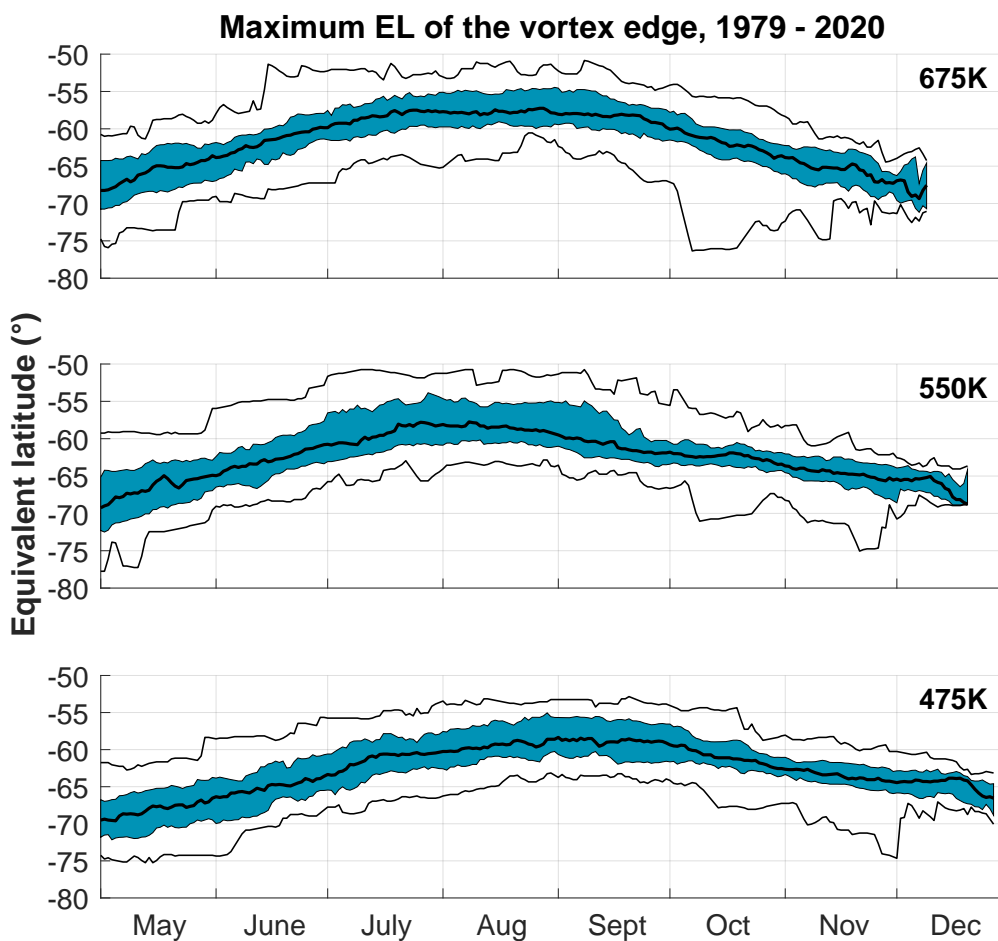
Figure 2. Evolution of daily maximum position of the vortex edge as a function of equivalent latitude over the 1979 - 2020 period, from top to bottom: 675K, 550K and 475K. Median values are represented by black bold curves. Blue filled areas show values between 20 and 80 percentiles, while thin black curves represent the maximum and minimum values over the period.

4.2 Influence of Solar Cycle, Quasi-Biennial Oscillation and El Niño Southern Oscillation on the polar vortex edge

Proxies such as the solar cycle, QBO and ENSO are used to describe the polar vortex edge interannual variation over the 1979
5 - 2020 period. As mentioned in the introduction, these variables were largely used in various studies of stratospheric polar vortices.

4.2.1 The Solar Cycle

The intensity of the vortex edge has been sorted according to the maximum (maxSC) and minimum (minSC) solar activity years (see section 2). Figure 3 displays the composite analysis of the temporal evolution of the polar vortex edge intensity throughout the winter from 1979 to 2020 at the three isentropic levels. In each panel, the dark (light) grey area represents

5   values between 20th and 80th percentiles of maxSC (minSC) years with the median in red (blue). The various panels of the figure show that minSC years are generally characterized by a stronger vortex edge. Also, maxSC years vortices break up earlier than during minSC, e.g. 6 days earlier at 675K, 4 days at 550K, and 3 days at 475K. The relative difference between the maxSC and minSC medians in the periods of maximum intensity is larger at 550K (16.4% relative difference) than at 475K (13%), and 675K (11.2%) levels. A t-test was performed to characterize the significance of these differences. Results

10   indicate that differences are significant from mid-September to the end of October with a mean p-value of 0.023 at 675K, from September to late November with p-value of 0.032 at 550K, and during the same period with a p-value of 0.023 at 475K. For the three levels, there is a jump in the vortex edge intensity for the maxSC years during November, which is not observed for minSC years. These jumps in the medians are related to smaller number of years included in the statistical parameters due to earlier vortex breakup dates for maxSC years.
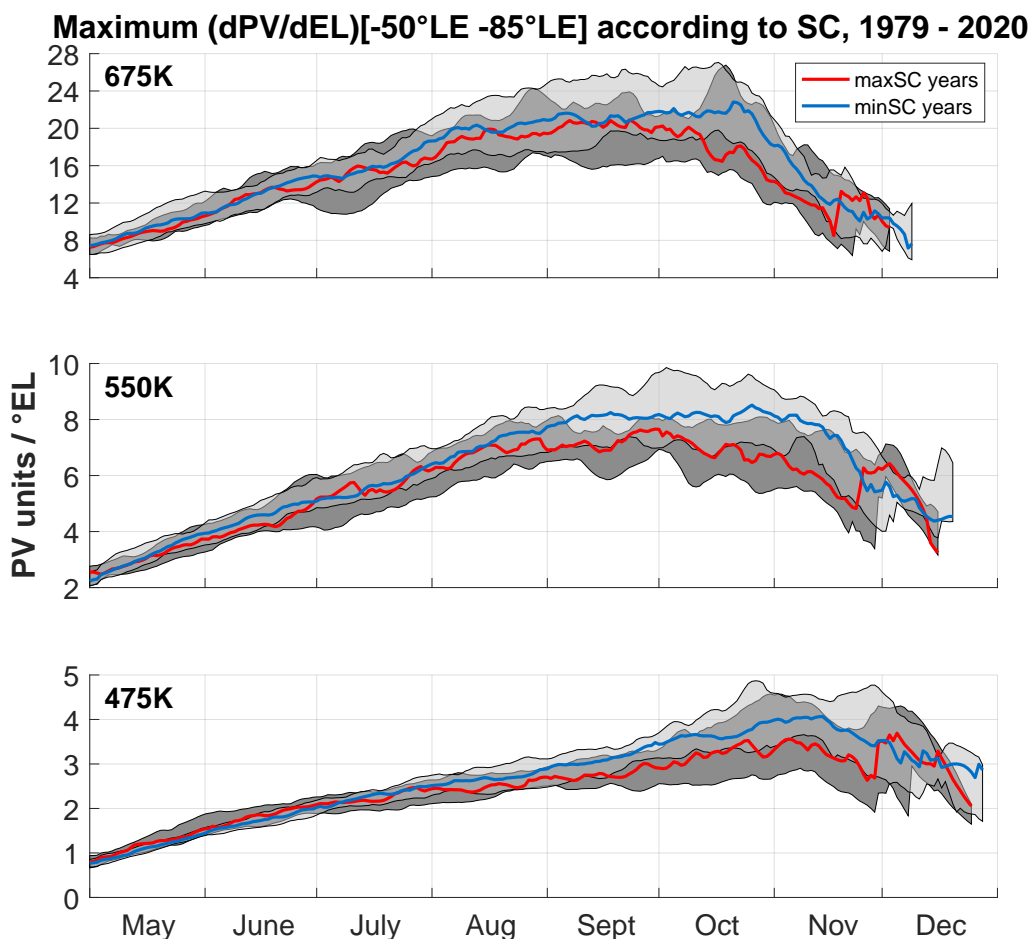
Figure 3. Composites of vortex edge intensity's annual evolution according to SC for the 1979 - 2020 period, from top to bottom: 675K, 550K and 475K. Red (blue) curves represent median values for maxSC (minSC) years. Dark (light) grey-filled areas indicate values between 20 and 80 percentiles for maxSC (minSC) years.

Figure 4 represents the statistical evolution of the vortex edge position according to SC in a similar way as in Figure 3 for the vortex edge intensity. Results do not show a large impact of the SC on the vortex edge position, although the vortex appears to be somewhat larger during maxSC periods, with also a larger variability. In the beginning of May, the vortex edge extends to -68°EL, then reaches a maximum at -56.1°EL (-57.4°EL) during the maxSC (minSC) between late August and mid-September at 675K. At 550K and 475K, maximum equivalent latitude positions reached according to the maxSC (minSC) years are -55.2°EL (-58.7°EL) between mid-July and August and -56.4°EL (-58.6°EL) between mid-August and September. There is less variability and fewer differences between maxSC and minSC years during the period of maximum intensity of the edge (see section 4.1). Differences between the medians are largest during the July - August period at 550K with a mean p-value of 0.03.
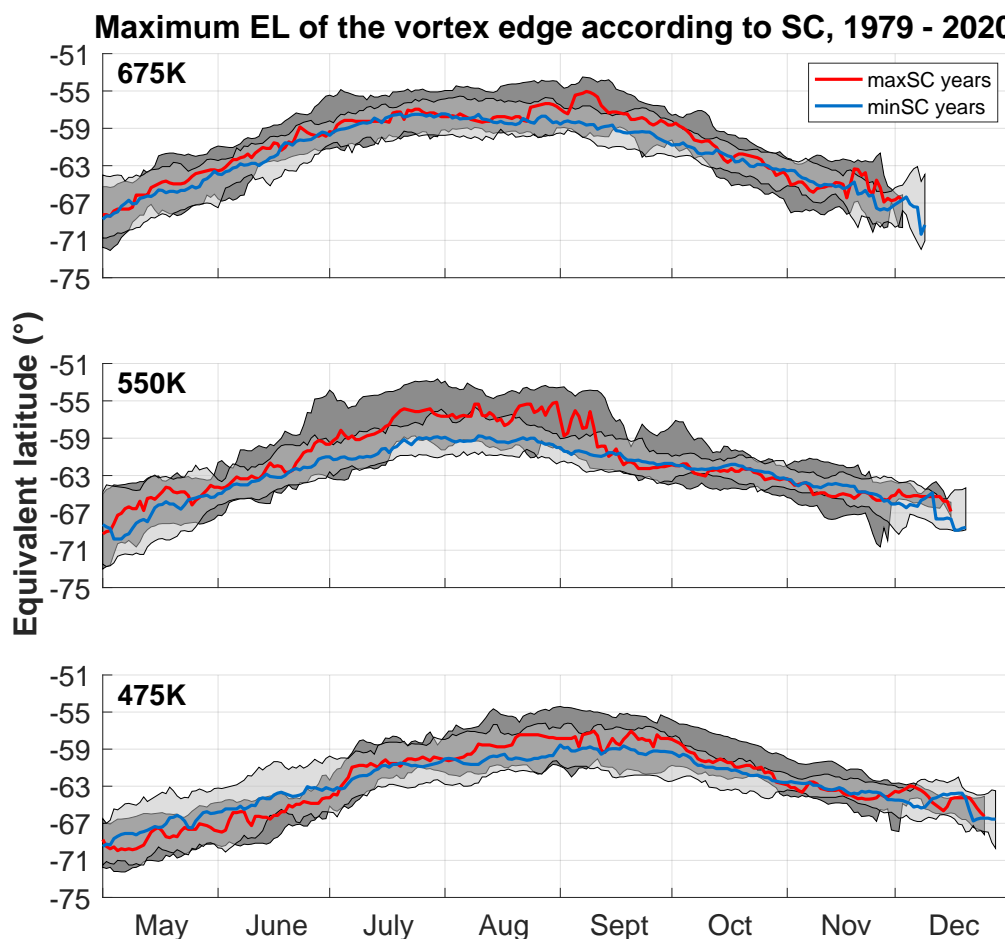
Figure 4. Composites of vortex edge position's annual evolution according to SC for the 1979 - 2020 period, from top to bottom: 675K, 550K and 475K. Red (blue) curves represent median values for maxSC (minSC) years. Dark (light) grey-filled areas indicate values between 20 and 80 percentiles for maxSC (minSC) years.

4.2.2 Quasi-Biennial Oscillation

We have then studied the modulation of the SC influence on the vortex edge by the QBO. Figure 5 represents the composite analysis of the polar vortex edge intensity throughout the winter for the 1979 - 2020 period at 550K and 475K, with maxSC and minSC years sorted with respect to the phase of the QBO: eQBO and wQBO are in the left and right panels respectively.

5 Only results for the lower levels are shown, as the differences are less clear at 675K. In each panel, the dark (light) grey area indicates the 20th and 80th percentiles of maxSC (minSC) years with the median in red (blue). Note that during the studied period there is only 5 years for maxSC/eQBO versus 10 years for minSC/eQBO, and 10 years for both maxSC/wQBO and minSC/wQBO. These results are synthetized in Table 2 for the solar cycle/QBO composite analysis.

At 550K, both QBO phases are characterized by a stronger vortex edge during minSC years but the differences between minSC and maxSC medians is largest during eQBO years. Largest variability of vortex edge intensity for minSC years (with largest observed values) is also seen for eQBO years. During wQBO phase, minSC years show a larger duration of the period of maximum intensity (from September to November) and maxSC years are characterized by a stronger vortex edge and a

5 longer vortex duration, compared to their equivalent during eQBO phases. A similar behavior of the vortex edge intensity is observed at 475K. MinSC and maxSC years show respectively stronger vortex edge intensity during wQBO phase than during eQBO phase. MaxSC years are characterized by a longer vortex duration during wQBO phase than during eQBO phase. As a conclusion, the QBO further modulates the intensity of the vortex edge, especially for maxSC years, which are generally characterized by a stronger vortex edge and longer vortex duration during wQBO phase than during eQBO phase. MinSC

10 years show also a slightly stronger vortex edge during wQBO phase.
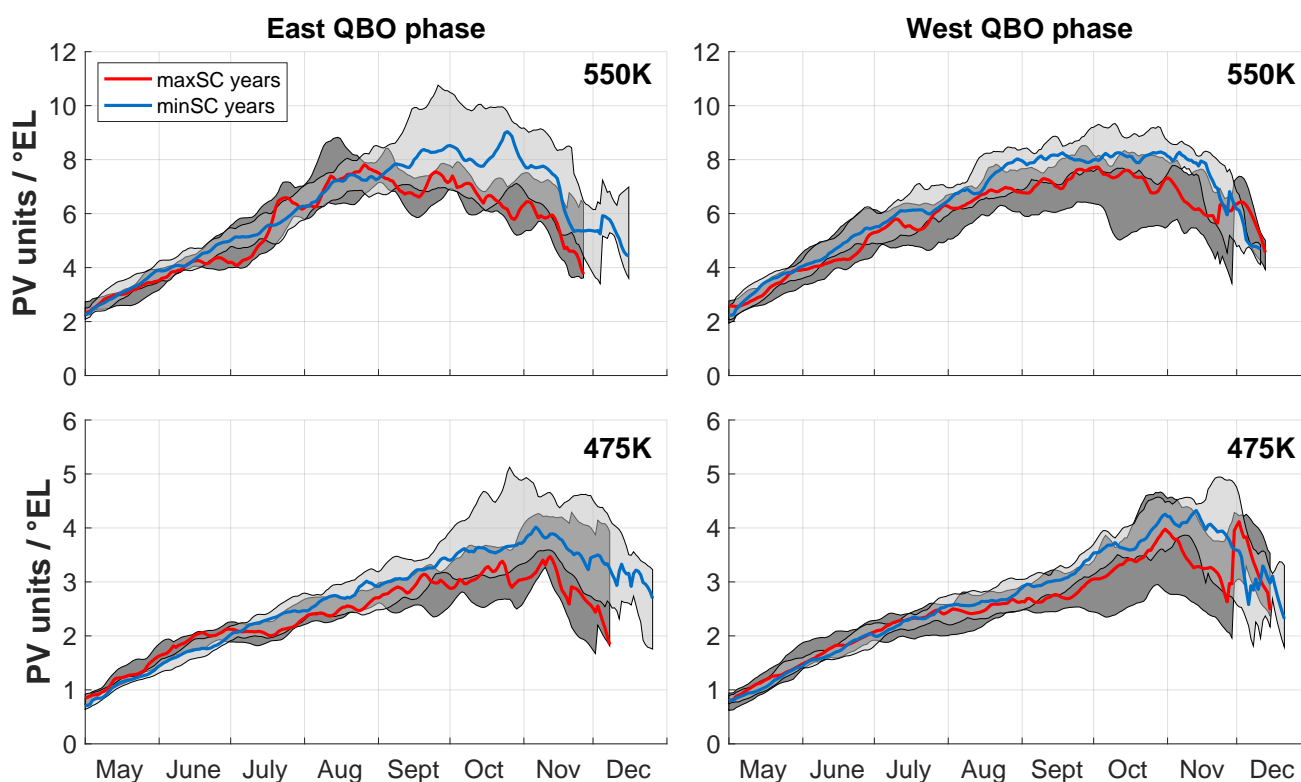
Figure 5. Composites of vortex edge intensity's annual evolution according to SC and QBO for the 1979 - 2020 period, from top to bottom: 550K and 475K. Left (rigth) panels represents eQBO (wQBO) phases. Red (blue) curves represent median values for maxSC (minSC) years. Dark (light) grey-filled areas indicate values between 20 and 80 percentiles for maxSC (minSC) years.

4.2.3 El Niño Southern Oscillation

We have also studied the combined modulation of the polar vortex edge by both the SC and ENSO. Figure 6 displays similar composites as in Figure 5 but selecting warm (wENSO) and cold (cENSO) ENSO phases (see section 2).

At both 550K and 475K, the largest difference between minSC and maxSC median vortex edge intensity is observed for
5 cENSO years, with minSC years still characterized by the largest intensity. MaxSC year's vortex duration is also larger during cENSO than wENSO years. At both levels, the difference between maxSC and minSC vortex edge intensity is small and insignificant during wENSO years, while cENSO are generally characterized by stronger vortex edge for both minSC and maxSC years.
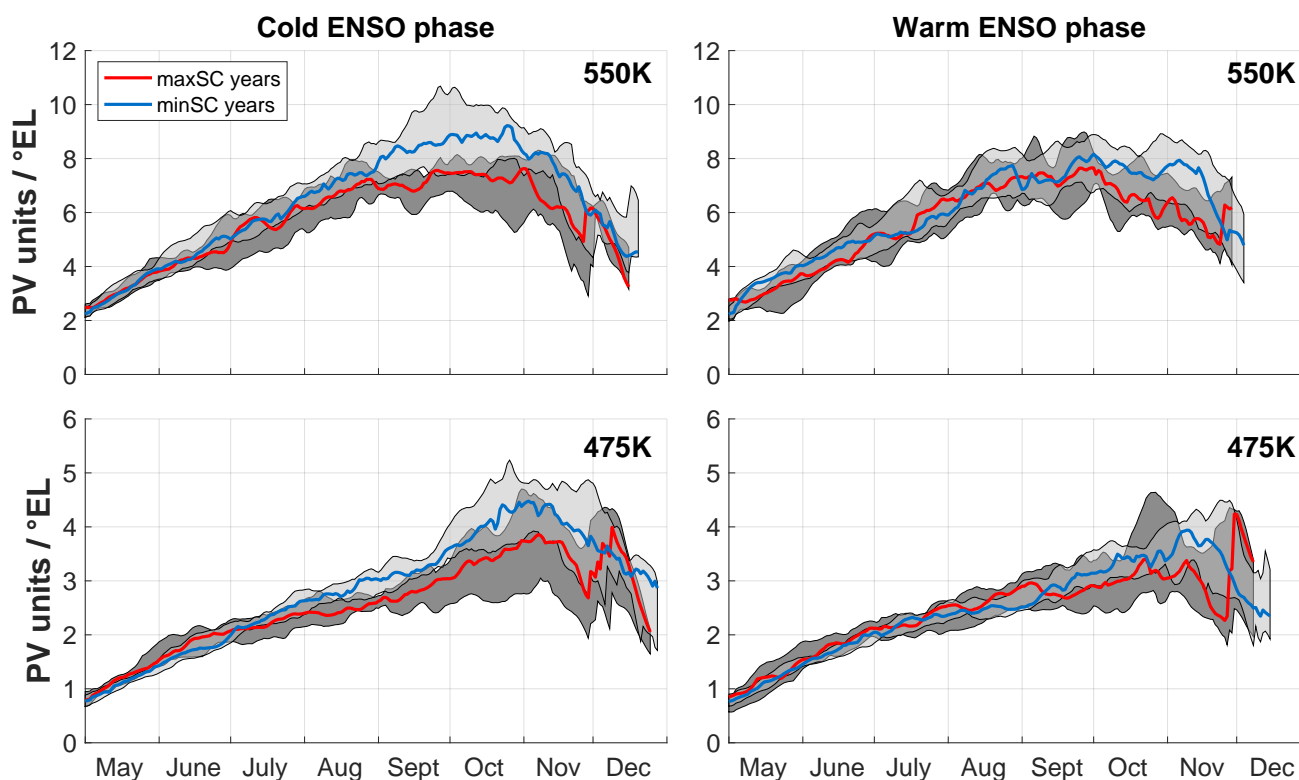
Figure 6. Composites of vortex edge intensity annual evolution according to SC and ENSO for the 1979 - 2020 period, from top to bottom: 675K, 550K and 475K. Left (rigth) panels represents cENSO (wENSO) phases. Red (blue) curves represent median values for maxSC (minSC) years. Dark (light) grey-filled areas indicate values between 20 and 80 percentiles for maxSC (minSC) years.

Table 2. Summary of the number of years considered in the composites analyses with SC, QBO and ENSO

Proxies	eQBO	wQBO	cENSO	wENSO
maxSC	5	10	8	7
minSC	10	10	11	9

4.3 Inter-annual evolution of the Polar Vortex edge

As seen in section 4.1, the maximum median intensity is reached from September to late October at 675K, from September to early November at 550K, and early November at 475K. In order to study the interannual evolution of the maximum intensity and position of the vortex edge during these periods, we identified the day when the maximum was reached at each level and

5 averaged the parameters over ±15 days around this date. Figure 7 represents the inter-annual evolution of the polar vortex edge maximum intensity at each isentropic level over the 1979 - 2020 period, averaged over September 15 – October 15, October and October 15 – November 15 at 675K, 550K and 475K respectively. Red circles (blue squares) indicate maxSC (minSC) years. Symbols-free years are years with 10.7-cm SF values in between minSC or maxSC years.

At 550K and 475K, an increase of the vortex edge intensity from the beginning of the period up to the end of the 1990s is

10 visible while this increase is not observed at 675K. It is about 121% and 136% at 550K and 475K respectively between 1980 and 1996, and about 61% and 86% between 1980 and 2000 at the same levels. This increase can be attributed to the increased formation of the ozone hole during the 1980s and 1990s as mentioned in other studies (Bodeker et al., 2002). From 2000, the intensity remains at a high level due to the continuing appearance of the ozone hole. Superimposed is the medium-term variability linked to the SC and inter-annual variability linked to the QBO and ENSO. In agreement with results in section 4.1

15 and 4.2, peaks observed around 1986, 1996, 2005 and 2016 are the signature of the 11-year solar cycle corresponding to minSC years. We note however that some maxSC years show high vortex edge intensity values, as e.g. 2014 at both 550K and 475K levels. This year is in west QBO phase, which confirms the previous conclusion that vortex edge intensity of maxSC years is stronger during wQBO phases. However, it is in warm ENSO phase, while it was shown that the maxSC median vortex edge intensity was lower during wENSO than during cENSO. It should be noted that the latest solar cycle (cycle number 24) was

20 less intense than the previous ones and the maxSC years of the last cycle correspond to intermediate years between minimum and maximum years of the previous cycles so the modulation of the vortex edge intensity by the latest solar cycle is potentially weaker than by the earlier cycles. Similarly, while years with low edge intensity generally correspond to maxSC years, minSC years also show low vortex intensity of the vortex edge especially at the end of the period (2016 - 2020), which corresponds to the end of the last weaker solar cycle.
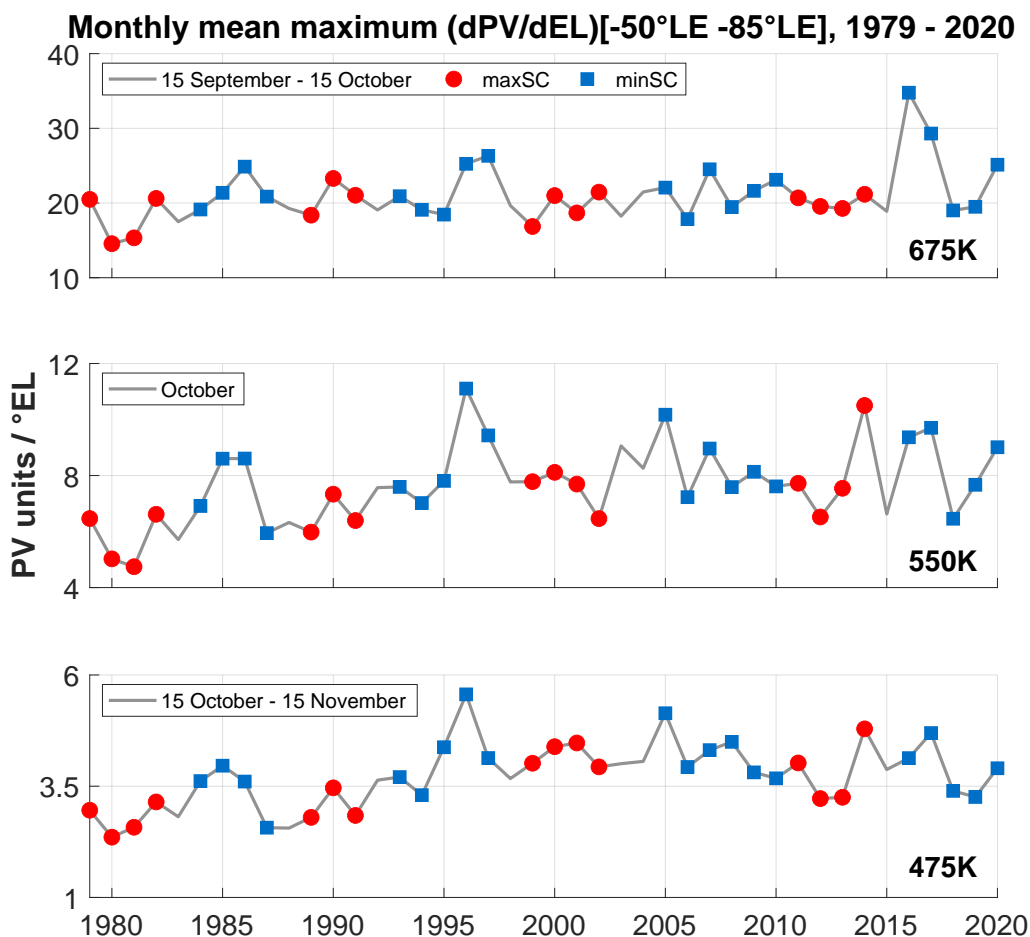
Figure 7. Inter-annual evolution of the maximum vortex edge intensity for the 1979 - 2020 period, averaged over September 15 – October 15 period for 675K, October for 550K, and the October 15 - November 15 period for 475K. MaxSC (minSC) years are represented by red circles (blue squares).

Figure 8 represents the inter-annual evolution of the maximum polar vortex edge position with years sorted according to the SC as described in Figure 7. The position of the vortex edge is quite similar for 550K and 475K levels. Between 1979 and 2001, the edge position is larger at 675K. The most noticeable feature in the Figure is the small edge position in 2002 due to the major warming and the vortex split, which occurred during that year. It was shown that the major warming in 2002, the first one observed over Antarctica, was mainly due to increased planetary waves activities in the southern stratosphere (Hoppel et al., 2003). Aside for this year, the maximum edge position fluctuates between -65.7°EL and -55.3°EL, all levels combined. At 550K and 475K levels, the edge position decreases from 1981 to 1994, with values varying from -56.6°EL and -58.6°EL to -63.4°EL and -63.7°EL respectively at both levels (average decrease of 7°EL to 5°EL in 14 years). It can be noted that these years correspond to the period when the intensity of the vortex edge increases. At 675K, the downward trend is less visible

during the first period. At all levels, particularly at 675K and 475K, there is a decrease in the edge size of the 2019 polar vortex which is due to the anomalously small ozone hole caused by a minor sudden stratospheric warming (Wargan et al., 2020). In contrast, the year 2020, which was characterized by a strong ozone hole and a very long vortex duration (see section 5) does not show a particularly strong maximum vortex edge intensity value nor an outstanding value of the edge position.
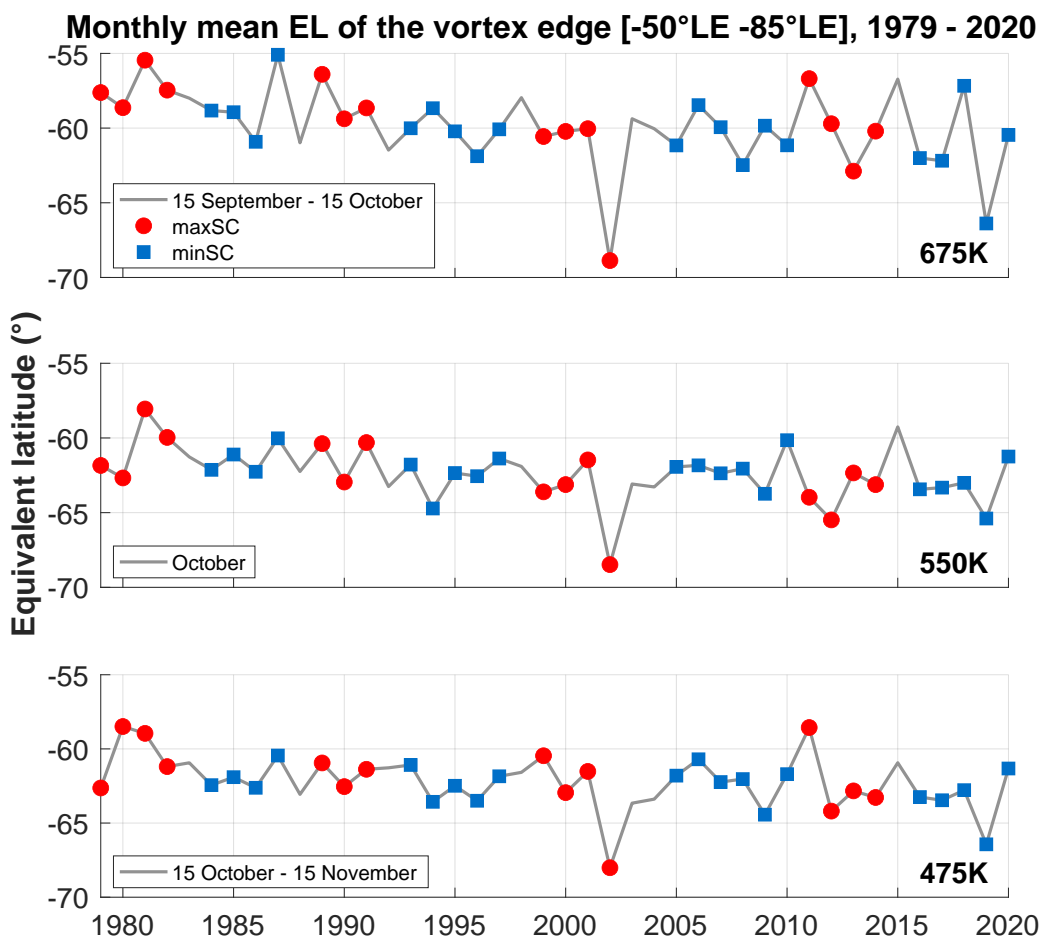
Figure 8. Inter-annual evolution of the maximum vortex edge position for the 1979 - 2020 period, averaged over September 15 – October 15 period for 675K, October for 550K, and the October 15 - November 15 period for 475K. MaxSC (minSC) years are represented by red circles (blue squares).

5 Onset and breakup of the Polar Vortex

The evolution of onset dates of the polar vortex throughout the winter from 1979 to 2020 at the 675K, 550K and 475K isentropic levels is displayed in Figure 9. It represents the day of the year when the polar vortex is well formed, e.g. when the horizontal wind speed at the vortex edge is above the threshold values of 15.2 m.s^{-1}, 20 m.s^{-1} and 25 m.s^{-1} as suggested by Akiyoshi

et al. (2009). In each panel, the blue, dark grey and light grey curves represent onset dates for the 15.2 m.s^{-1}, 20 m.s^{-1} and 25 m.s^{-1} thresholds respectively.

As expected, the vortex forms earlier at the highest levels: the average day of the year the onset date occur for all thresholds combined is on days 90, 98 and 108 at 675K, 550K and 475K respectively. Also, the onset date occurs later for the larger

5 threshold values as the wind strength increases in Autumn in the polar stratosphere. The differences between onset dates according to the different threshold values decreases with altitude. At 475K, mean values of the onset dates are days 93, 109 and 125 for the 15.2 m.s^{-1}, 20 m.s^{-1} and 25 m.s^{-1} thresholds respectively. However, some years show large difference between the onset dates according to the different threshold values, which can exceed one month (for example in 2002 with one and a half month between 15.2 m.s^{-1} and 25 m.s^{-1}). This year was however characterized by the first major warming

10 observed in Antarctica, as mentioned previously. Also, the inter-annual variability of onset dates is rather important at this level, with an average day difference of 32.9 days between 15.2 m.s^{-1} and 25 m.s^{-1} during the whole period. There are some outstanding late onset dates at 475K, particularly for the 25 m.s^{-1} threshold, e.g. on day 152 in 2002 and day 149 in 2014. In contrast the year 1992 was characterized by an early onset on day 73 for the 15.2 m.s^{-1} threshold. The 550K and 675K levels show comparatively less variability of the onset dates for the various threshold values and the difference between the onset

15 dates for the largest and lowest threshold values is of the order of 10 days in average (21 and 17.2 days at 550K and 675K respectively between the 25 m.s^{-1} and 15.2 m.s^{-1} threshold values). This difference in inter-annual variability of the onset among the levels is further confirmed from the standard deviation average of the three thresholds curves after corrected from long-term variation by a 3-degree polynomial. This standard deviation amount to ±8.2 days at 475K, which is almost twice larger than the values of the 675K and 550K levels (±4.8 and ±3.7 days respectively).

20 Some long-term variability in the evolution of the onset dates is also observed at the different levels. At 675K, a decreasing trend is visible between 2010 and 2018 for the 15.2 m.s^{-1} threshold, with a slightly higher inter-annual variability during this last decade. At 550K a similar decrease of the onset date from 2011 is observed, most pronounced for the 15.2 m.s^{-1} threshold. At 475K, the most prominent feature is a significant decline of the onset dates between 1980 and 1999 for the 25 m.s^{-1} threshold value of about 29 days in 19 years, corresponding to a decline of 1.5 days per year. It is remarkable also to

25 notice that later onset days in 2002, 2012 and 2014, correspond to years with smaller ozone holes (e.g. Pazmino et al., 2018).
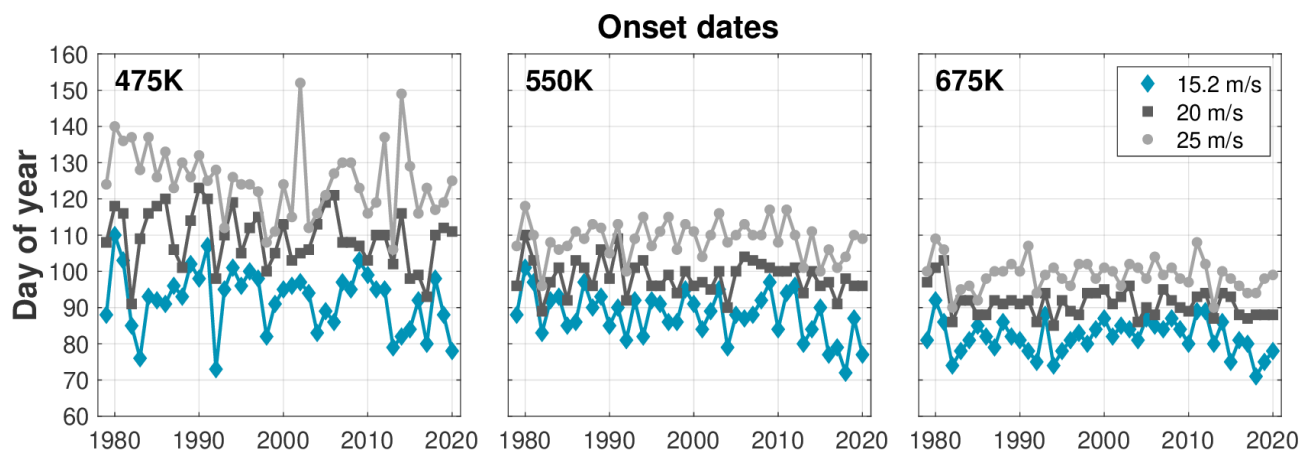
Figure 9. Interannual evolution of Antarctic polar vortex onset dates over the 1979 - 2020 period. Panels from left to right show onset dates at 475K, 550K and 675K. Light grey, dark grey and blue curves represent onset dates for the 15.2 m.s^{-1}, 20 m.s^{-1} and 25 m.s^{-1} wind threshold values (see text).

Similarly, as in Figure 9, Figure 10 shows the day when the polar vortex breaks up in Spring due to the final vortex warming, at 475K, 550K and 675K isentropic levels. As mentioned in Nash et al. (1996), when the vortex is weakening between early and late Spring, the winds at the vortex edge also weaken, leading to the final vortex breakup. The vortex breakup is thus considered to occur when the horizontal wind speed along the vortex edge falls below the 15.2 m.s^{-1}, 20 m.s^{-1} or 25 m.s^{-1}

5 threshold values.

The vortex forms earlier at the highest levels and it also breaks earlier: the average breakup dates for the different threshold values are on days 340, 334 and 325 at 475K, 550K and 675K respectively. We notice some early breakup of the polar vortex: for example, in 1988 the vortex broke up 13 days before the mean breakup date at 675K, 20 days at 550K and 21 days at 475K. In 2002, the breakup occurred 18, 9 and 8 days before the mean breakup date at 475K, 550K and 675K respectively. Some late

10 breakups are observed during the last two decades particularly at 15.2 m.s^{-1}. The year 1999 is clearly noticeable at 475K and 550K with respectively 21 and 27 days after the mean breakup date for this threshold value. The years 2007, 2008, 2010 and 2015 also stand out for the three levels: around 14 days, 15 days and 14 days after the mean breakup date at 475K, 550K and 675K respectively. Finally, the year 2020 is noticeable for its exceptionally late breakup date, with an average breakup for the three thresholds on days 360, 355 and 354 at 475K, 550K, and 675K, respectively. The latter value sets a record over the whole

15 studied period for the 675K level.

The Figure shows that the difference between the breakup dates for the various threshold value is much smaller than for the onset dates. The average difference between breakup dates for 15.2 m.s^{-1} and 25 m.s^{-1} is equal to 11.5, 8.9 and 8.2 days at 475K, 550K and 675K respectively, compared to $\pm$32.9, $\pm$21 and $\pm$17.2 days respectively for the onset dates. This smaller difference can be explained by the important role played by dynamical processes in the vortex breakup while the

20 vortex formation is mainly controlled by radiative processes that are less variable from one year to the next. A larger inter-

annual variability is also observed for the breakup dates at the various levels and threshold values. Similarly, as for the onset dates, we calculated the standard deviation over the period after averaging the different curves of the different threshold mean. and removing the long-term trend by a 3-degree polynomial. The standard deviation is equal to 10.6, 10.2 and 10.4 days at 475K, 550K and 675K respectively, compared to 8.2, 4.8 and 3.7 days for onset dates.

5   An increasing trend of the breakup dates between 1979 and 1999 is seen at all levels, which is more pronounced at 475K. It corresponds to 35, 30 and 15 days over 21 years at 475K, 550K and 675K respectively, if we average the different threshold values at the various levels. The vortex is thus persisting later after 1999. For all levels, another trend was visible, corresponding to a decrease from 2000, which was halted by the very long duration of the 2020 polar vortex. While late breakup dates in December were already observed at 475K and 550K, as mentioned previously the vortex duration up to day 354 was exceptional

10   at 675K.
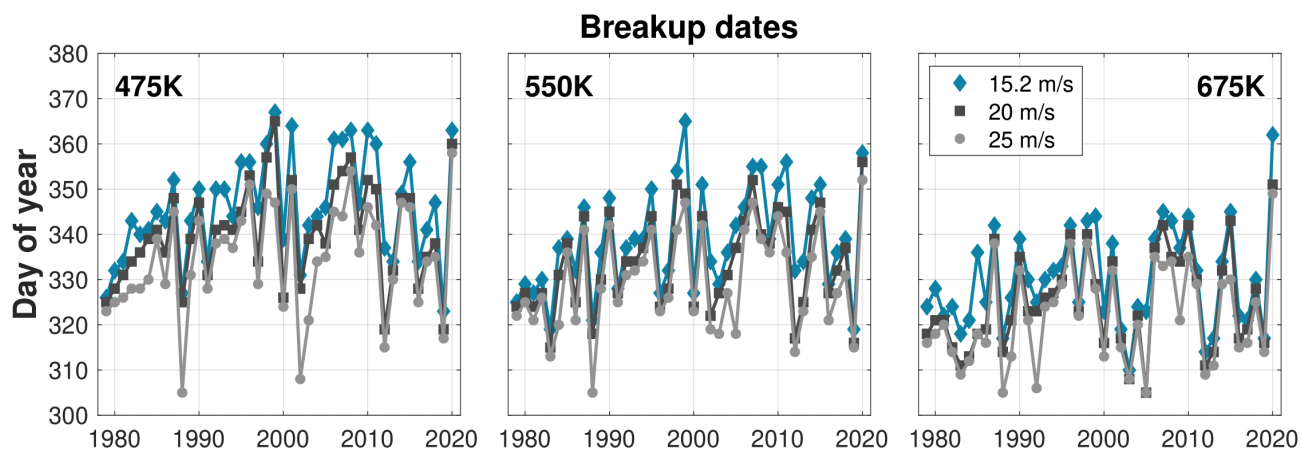
Figure 10. Interannual evolution of Antarctic polar vortex breakup dates over the 1979 - 2020 period. Panels from left to right show onset dates at 475K, 550K and 675K. Light grey, dark grey and blue curves represent onset dates for the 15.2 m.s^{-1}, 20 m.s^{-1} and 25 m.s^{-1} wind threshold values.

Table 3. Summary of the onset and breakup dates

		675K	550K	475K
Onset	Average onset day over the period and for the 3 thresholds	90	98	108
	Mean difference on the period between 25 m.s^{-1} and 15.2 m.s^{-1}	17.2	21	32.9
	Std of average threshold dates after long-term trend corrected	3.7	4.8	8.2
Breakup	Average breakup day over the period and for the 3 thresholds	325	334	340
	Mean difference on the period between 25 m.s^{-1} and 15.2 m.s^{-1}	11.5	8.9	8.2
	Std of average threshold dates after long-term trend corrected	10.4	10.2	10.6

6   Conclusion and perspectives

We have analyzed the seasonal evolution of the stratospheric polar vortex edge intensity and position as a function of equivalent latitude in the Southern hemisphere at three isentropic levels, using ECMWF data over the 1979 - 2020 period. The inter-annual evolution of the maximum vortex edge intensity and position, as well as the onset and breakup dates at these three isentropic

5   levels were evaluated. The vortex edge intensity corresponds to the gradient of the potential vorticity weighted by the wind module as a function of equivalent latitude (Nash et al., 1996). The studied parameters display long-term and short-term variations over the period that were analyzed using well known proxies of atmospheric variability in the stratosphere such as the solar cycle, the QBO and ENSO. Among the main results of our study, the influence of increasing ozone hole during the 1980s and 1990s on the studied parameters was clearly noticeable, confirming the results of Bodeker et al. (2002). This

10   influence is mostly pronounced on the maximum intensity of the vortex edge, with an increase of 0.38 PV units/°EL per year at 550K and 0.30 PV units/°EL per year at 475K between 1980 and 1996. It is also visible on the vortex breakup dates with an increasing trend of respectively 1.75 days.yr^{-1}, 1.5 days.yr^{-1} and 0.75 days.yr^{-1} at 475K, 550K and 675K levels, for the average threshold values over the 1979 - 1999 period. We also find a decreasing trend over the same period for the onset dates but in this case only at 475K, and for the 25 m.s^{-1} threshold value only (1.5 days.yr^{-1} between 1980 and 1999). A seemingly

15   decreasing trend in the breakup dates after 2010 was halted by the very long vortex duration in 2020, which set a record at the 675K level. The solar cycle and to a lower extent the QBO and ENSO modulate the inter-annual evolution of the maximum intensity of the vortex edge and the breakup dates. Stronger vortex edge intensity is observed in years of solar minimum. QBO and ENSO further modulate the solar cycle influence on the vortex edge, especially at 475K and 550K: during wQBO phases, the difference between vortex edge intensity for minSC and maxSC years is smaller than during eQBO phases. The polar vortex

20   edge is stronger and lasts longer for maxSC/wQBO than for maxSC/eQBO. Regarding ENSO, which has a lower impact than the QBO, the vortex edge intensity is somewhat stronger during cENSO phases for both minSC and maxSC, and the difference between minSC and maxSC medians is larger.

These results are mainly in agreement with the literature. Baldwin and Dunkerton (1998) found that the strongest influence of the QBO on the southern polar vortex occurs in late spring (November) when the final warming happens. From tempera-

25   ture composites at 10hPa, they found that the vortex is slightly colder during the western phase of the QBO throughout the winter. Later, Haigh and Roscoe (2009) found that the southern stratospheric polar vortex breaks down later for combined maxSC/wQBO and minSC/eQBO years. The last two years of the study (2019 and 2020) stand out in our analysis. In 2019, the vortex maximum area was particularly small, especially at 475K and 675K and the vortex broke up quite early. The breakup date at 475K and 550K for the 15 m.s^{-1} threshold is the lowest on record (on day 323 at 475K and 319 at 550K). In 2020,

30   the vortex area was not particularly large and the vortex edge not particularly strong but its duration set a record at 675K. This very long-lasting vortex was also characterized by a strong ozone destruction (https://public.wmo.int/en/media/news/2020-antarctic-ozone-hole-large-and-deep and https://public.wmo.int/en/media/news/record-breaking-2020-ozone-hole-closes). It will be interesting to see how the southern polar vortex will evolve in the coming years.

A major perspective of our study is to extend the period analysis, using ERA5 reanalyses which are covering a longer period (from 1950) and with a higher resolution (https://www.ecmwf.int) (31km grid for ERA5 versus 79km for ERA-Interim). The same parameters for the more widely studied Arctic polar vortex are currently being studied for comparison between the two hemispheres. Other factors, which particularly influence the northern hemisphere, such as the Arctic Oscillation/Northern

5 Annular Mode, will be included in the study.

Data availability. The data that support the findings of this study are openly available in [1] ECMWF ERA-Interim https://www.ecmwf.int/en/forecasts/datasets/reanalysis-datasets/era-interim [2] Solar flux at 10.7-cm ftp://ftp.seismo.nrcan.gc.ca/spaceweather/solar_flux/monthly_averages/solflux_monthly_average.txt, last access: 11 May 2021 [3] https://www.geo.fu-berlin.de/met/ag/strat/produkte/qbo/qbo.dat, last access: 11 May 2021 [4] https://www.esrl.noaa.gov/psd/enso/mei, last access: 11 May 2021. The code for the determination of the vortex edge

10 intensity and position is available upon request to A. Lecouffe (audrey.lecouffe@latmos.ipsl.fr)

Author contributions. A. Lecouffe made the study and provided the results. All authors discussed the results and contributed to the final paper.

Competing interests. The authors declare that they have no conflict of interest.

Acknowledgements. The authors wish to thank Cathy Boone of Institut Pierre Simone Laplace (IPSL) for providing ERA-Interim data, and

15 ECMWF for the availability of these data.

References

Akiyoshi, H., Zhou, L., Yamashita, Y., Sakamoto, K., Yoshiki, M., Nagashima, T., Takahashi, M., Kurokawa, J., Takigawa, M., and Imamura, T.: A CCM simulation of the breakup of the Antarctic polar vortex in the years 1980–2004 under the CCMVal scenarios, Journal of Geophysical Research: Atmospheres, 114, 2009.

5   Baldwin, M. P. and Dunkerton, T. J.: Quasi-biennial modulation of the southern hemisphere stratospheric polar vortex, Geophysical Research Letters, 25, 3343–3346, 1998.

Bodeker, G., Struthers, H., and Connor, B.: Dynamical containment of Antarctic ozone depletion, Geophysical research letters, 29, 2–1, 2002.

Butchart, N. and Remsberg, E. E.: The area of the stratospheric polar vortex as a diagnostic for tracer transport on an isentropic surface,
10   Journal of the atmospheric sciences, 43, 1319–1339, 1986.

Dee, D. P., Uppala, S. M., Simmons, A., Berrisford, P., Poli, P., Kobayashi, S., Andrae, U., Balmaseda, M., Balsamo, G., Bauer, d. P., et al.: The ERA-Interim reanalysis: Configuration and performance of the data assimilation system, Quarterly Journal of the royal meteorological society, 137, 553–597, 2011.

Farman, J. C., Gardiner, B. G., and Shanklin, J. D.: Large losses of total ozone in Antarctica reveal seasonal ClOx/NOx interaction, Nature,
15   315, 207, 1985.

Godin, S., Bergeret, V., Bekki, S., David, C., and Mégie, G.: Study of the interannual ozone loss and the permeability of the Antarctic polar vortex from aerosol and ozone lidar measurements in Dumont d'Urville (66.4 S, 140 E), Journal of Geophysical Research: Atmospheres, 106, 1311–1330, 2001.

Gray, L. J.: The influence of the equatorial upper stratosphere on stratospheric sudden warmings, Geophysical research letters, 30, 2003.

20   Haigh, J. D. and Roscoe, H. K.: The final warming date of the Antarctic polar vortex and influences on its interannual variability, Journal of climate, 22, 5809–5819, 2009.

Hauchecorne, A., Godin, S., Marchand, M., Heese, B., and Souprayen, C.: Quantification of the transport of chemical constituents from the polar vortex to midlatitudes in the lower stratosphere using the high-resolution advection model MIMOSA and effective diffusivity, Journal of Geophysical Research: Atmospheres, 107, SOL–32, 2002.

25   Heese, B., Godin, S., and Hauchecorne, A.: Forecast and simulation of stratospheric ozone filaments: A validation of a high-resolution potential vorticity advection model by airborne ozone lidar measurements in winter 1998/1999, Journal of Geophysical Research: Atmospheres, 106, 20 011–20 024, 2001.

Holton, J. R. and Tan, H.-C.: The influence of the equatorial quasi-biennial oscillation on the global circulation at 50 mb, Journal of Atmospheric Sciences, 37, 2200–2208, 1980.

30   Hoppel, K., Bevilacqua, R., Allen, D., Nedoluha, G., and Randall, C.: POAM III observations of the anomalous 2002 Antarctic ozone hole, Geophysical research letters, 30, 2003.

Labitzke, K. and Van Loon, H.: Associations between the 11-year solar cycle, the QBO and the atmosphere. Part I: the troposphere and stratosphere in the northern hemisphere in winter, Journal of Atmospheric and Terrestrial Physics, 50, 197–206, 1988.

Manney, G., Zurek, R., Gelman, M., Miller, A., and Nagatani, R.: The anomalous Arctic lower stratospheric polar vortex of 1992–1993,
35   Geophysical research letters, 21, 2405–2408, 1994.

McIntyre, M. E. and Palmer, T.: Breaking planetary waves in the stratosphere, Nature, 305, 593–600, 1983.

Millan, L. F., Manney, G. L., and Lawrence, Z. D.: Reanalysis intercomparison of potential vorticity and potential-vorticity-based diagnostics, Atmospheric Chemistry and Physics Discussions, pp. 1–34, 2020.

Mishra, V., Tiwari, D., Tiwari, C., and Agrawal, S.: Comparative study of different solar parameters with sunspot numbers, 96.60 Rd: 96.60 Qe, 2005.

5 Nakamura, N.: Two-dimensional mixing, edge formation, and permeability diagnosed in an area coordinate, Journal of the atmospheric sciences, 53, 1524–1537, 1996.

Nash, E. R., Newman, P. A., Rosenfield, J. E., and Schoeberl, M. R.: An objective determination of the polar vortex using Ertel's potential vorticity, Journal of Geophysical Research: Atmospheres, 101, 9471–9478, 1996.

NOAA: This is how you cite a website in latex, https://www.cpc.ncep.noaa.gov/products/stratosphere/winter_bulletins/sh_06/, 2021.

10 Pazmino, A., Godin-Beekmann, S., Hauchecorne, A., Claud, C., Khaykin, S., Goutail, F., Wolfram, E., Salvador, J., and Quel, E.: Multiple symptoms of total ozone recovery inside the Antarctic vortex during austral spring, Atmospheric Chemistry and Physics, 18, 7557–7572, 2018.

Schoeberl, M. R. and Hartmann, D. L.: The dynamics of the stratospheric polar vortex and its relation to springtime ozone depletions, Science, 251, 46–52, 1991.

15 Solomon, S.: Stratospheric ozone depletion: A review of concepts and history, Reviews of Geophysics, 37, 275–316, 1999.

Tiwari, B. R. and Kumar, M.: The Solar Flux and Sunspot Number; A Long-Trend Analysis, International Annals of Science, 5, 47–51, 2018.

Wargan, K., Weir, B., Manney, G. L., Cohn, S. E., and Livesey, N. J.: The anomalous 2019 Antarctic ozone hole in the GEOS Constituent Data Assimilation System with MLS observations, Journal of Geophysical Research: Atmospheres, 125, e2020JD033 335, 2020.

Waugh, D. N.: Elliptical diagnostics of stratospheric polar vortices, Quarterly Journal of the Royal Meteorological Society, 123, 1725–1748,
20 1997.

Waugh, D. W. and Randel, W. J.: Climatology of Arctic and Antarctic polar vortices using elliptical diagnostics, Journal of the Atmospheric Sciences, 56, 1594–1613, 1999.

Waugh, D. W., Randel, W. J., Pawson, S., Newman, P. A., and Nash, E. R.: Persistence of the lower stratospheric polar vortices, Journal of Geophysical Research: Atmospheres, 104, 27 191–27 201, 1999.

25 WMO: (World Meteorological Organization), Scientific Assessment of Ozone Depletion: 2018, Global Ozone Research and Monitoring Project–Report No. 58, 588 pp., Geneva, Switzerland, Tech. rep., 2018.

WMO: (World Meteorological Organization), Statement on the State of the Global Climate in 2019, Project–Report No. 1248, 44 pp., Geneva, Switzerland, Tech. rep., 2019.

Zhou, S., Gelman, M. E., Miller, A. J., and McCormack, J. P.: An inter-hemisphere comparison of the persistent stratospheric polar vortex,
30 Geophysical research letters, 27, 1123–1126, 2000.